J Bio Tribo Corros (2015) 1:17
DOI 10.1007/s40735-015-0017-9

ORIGINAL PAPER

Pure Mechanical Wear Measurement of Carbon Steel in Oil–Water Fluids

Z. Y. Hu[1] · D. L. Duan[1] · S. L. Jiang[1] · X. J. Ding[1] · S. Li[1]

Received: 6 March 2015 / Revised: 9 May 2015 / Accepted: 12 May 2015 / Published online: 27 May 2015

Abstract The pure mechanical wear (PMW) component of the corrosive wear of carbon steel (CS) in oil–water fluids was investigated by surface morphology and composition analysis after tests. Negative potential protection method and sacrificial anode (SA) of Zn–Al–Cd and Mg–Mn were used to eliminate the corrosion effect in oil–water fluids with different flow patterns and explore the optimal program for the PMW research. The influences of the area ratios of SA to CS samples on the PMW behaviour of CS samples were also studied. Experimental results demonstrated that the system of oil–$NaHCO_3$ aqueous solution + SA of Mg–Mn was the best mean. The area ratio of SA to CS samples should be controlled within a proper range of 0.5–2.

Keywords Steel · Sliding wear · Surface analysis · Corrosive wear · Electrochemistry

1 Introduction

Water flooding is the primary technique for oil exploration in oil production. This approach enhances the efficiency of oil recovery but induces many corrosive wear problems of carbon steel (CS), which is widely employed in the oil industry, such as in sucker rods and production tubes. The shutdown of oil wells as a result of the repair and replacement of sucker rods and production tubes causes tremendous economic loss. Thus, many researchers have investigated the corrosive wear of CS in the oil industry. Ko [1] studied the effects of load, sliding rate and fluid composition on sucker rod/tube wear in large-scale and small-scale tests. The wear rate increased with the normal contact load and the sliding rate, and the wear rates were lower in an oil–water emulsion environment than in an aerated water environment. Zheng [2] simulated the actual working conditions of drill pipes to investigate the effects of Cl^-, S^{2-} and pH on the corrosion fatigue of CS in drilling fluids. The fatigue loss of CS was accelerated by pitting and hydrogen permeation induced by Cl^- and S^{2-}, respectively. However, the fatigue life of CS was lengthened when pH was increased. Our group [3] studied the corrosive wear behaviour of CS in oil–water fluid on the basis of surface wetting state. The corrosive wear behaviour of CS was related to the surface wetting film and surface reaction film.

To study the corrosive wear and find the predominant factor in the corrosive wear, corrosive wear loss has been divided into three parts, namely, loss caused only by chemical corrosion, loss caused only by mechanical wear and the synergistic loss of corrosion and wear [4–10]. The weight loss of CS under cathodic protection has been accepted as the pure mechanical wear (PMW) component in the corrosive environment. Cheng [11], Mischler [12] and Assi [4] claimed that the weight loss under the protection of impressed current could be considered as the PMW in corrosive media. Nevertheless, Cheng [11] pointed out that the existence of alternating current would dramatically decrease the cathodic protection efficiency. Jiang [13] and Akonkoa [7] found that corrosion could be limited under negative potential (NP) protection. Akonkoa [7] demonstrated that a high wearing force or considerable negative cathodic potential was not beneficial to the cathodic protection efficiency because of hydrogen embrittlement. Yaro

✉ D. L. Duan
duandl@imr.ac.cn

[1] Institute of Metal Research, Shenyang 110016, Liaoning, China

[14] and Shehadeh [15] found that sacrificial anode (SA) protection could be utilised to control corrosion in corrosive media and research the PMW component of corrosive wear, although the protection efficiency was affected by temperature, flow rate, pH and time.

However, almost all studies on the PMW component of corrosive wear have been conducted in an aqueous water solution, and the PMW study of CS in an oil–water condition has not attracted enough attention. The main factor that aggravates CS corrosive wear in oil–water fluids was difficult to determine because existing protection methods remain empirical and inefficient.

In this study, the PMW component of the corrosive wear of CS in oil–water fluids was investigated. SA and NP protection were applied to control CS corrosion. The efficiency of the two methods was inspected by surface morphology and surface elemental analysis of samples after tests. Meanwhile, in order to select the optimal protection system including cathode protection method and aqueous solution condition for the PMW study of CS in oil–water two-phase fluids, the effect of fluid patterns and the area ratios(r) of SA to the samples exposed in the fluids on the PMW behaviours were investigated. The best protection system should be used in oil–water fluids with three flow patterns, namely, oil-in-water (O/W), phase inversion point (PIP) and water-in-oil (W/O). Therefore, tests were conducted in three kinds of fluids until the best protection system could be selected. This study finds the best protection system and proper parameter for the CS PMW study in a white oil–water fluid and lays a foundation for the corrosive wear study of CS in oil–water fluids.

2 Experimental Work

2.1 Oil–Water Fluids

Skaln type 3 white oil, with a density of 832 kg/m^3, a viscosity of 2.88 mm^2/s and a surface tension of 27.27 mN/m at 25 °C, was selected as the oil phase of the oil–water fluid. NaCl and $NaHCO_3$ with a salinity of 3 % (wt%) and distilled water (DW) were chosen as the water phase. Experiments were conducted in white oil–water fluids with water contents of 5, 25 and 45 %, which represented W/O, PIP and O/W patterns according to the research results of fluid patterns of the oil–water mixture, respectively [16–20]. The fluid velocity during experiments was adjusted to 0.24 m/s.

2.2 Samples

The samples and frictional pairs were made of AISI 1045 CS with a chemical composition of (wt%) 0.45 C, 0.2 Si, 0.62 Mn, 0.22 Cr, 0.2 Ni, 0.05 Cu and balance Fe. They were machined with dimensions of 60 mm × 36 mm × 5 mm and 17 mm × Φ3 mm, respectively. To achieve uniform and adequate surface finish, all samples and frictional pairs were ground with a grinder and polished using a diamond polishing liquid with a particle size of 2.5 μm. They were then cleaned with anhydrous ethanol in an ultrasonic cleaner, dried, weighted by an electronic balance with a precision of 0.1 mg and stored in a desiccator. After the experiments, the samples were cleaned by DW and ethanol, dried and re-weighted to calculate weight loss. The experimental were conducted with a stroke length of 50 mm, stroke frequency of 60 min^{-1}, normal contact load of 100 N and testing span of 1 h.

2.3 Experimental Details

Experimental data were obtained using a pin on disc reciprocating tribocorrosion apparatus manufactured by Jinan Shunmao Test Instrument Limited Company. The schematic diagram of the apparatus is shown in Fig. 1. The sample 7 was mounted in a rectangle-shaped sample chamber 22, leaving a testing area of 60 mm × 5 mm, with the remaining surface sealed by tape. The sample chamber placed on the sample platform 6 was connected to the hydraulic press 8 below. The press could adjust the normal contact force by lifting the test sample platform to contact with the pin 14 until the predetermined value was reached. Four vertical transducers 5 and a horizontal transducer 16 were mounted beneath and on the side of the sample platform, respectively, to measure the normal and frictional forces. The pin was installed in a cylindrical holder 13 connected to the sliding rail 19. A SGMGV-

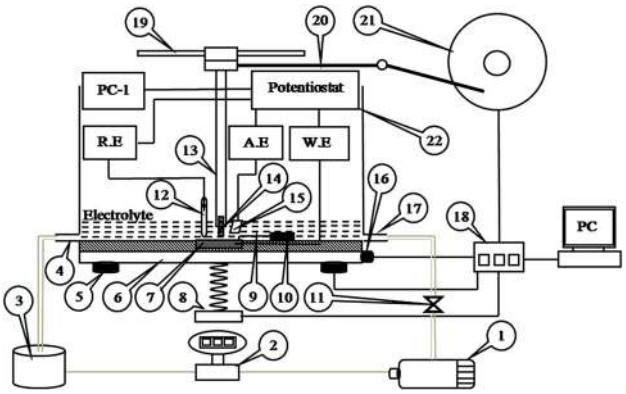

Fig. 1 Schematic of the reciprocating corrosive wear apparatus. *1*-Pump; *2*-oval gear volume flow metre; *3*-reservoir; *4*-outlet; *5*-normal force transducer; *6*-sample platform; *7*-sample; *8*-hydraulic machine; *9*-Cu wire; *10*-SA; *11*-flow rate control valve; *12*-salt bridge; *13*-holder; *14*-pin; *15*-Pt plate; *16*-friction force transducer; *17*-inlet; *18*-control cabinet; *19*-sliding rail; *20*-driving rod; *21*-motor; *22*-sample chamber

20ADA61 motor 21 with a rated power of 1.8 kW was connected to the pin holder by a driving rod 20 to provide reciprocating motion between the pin and the test sample. All the aforementioned operations were controlled and recorded by a computer (PC).

NP protection and SA protection were employed in the experiments to inhibit corrosion. NP protection was conducted via Potentiostat/Galvanostat Princeton MODEL 273 in a conventional three-electrode electrochemical cell. The CS sample worked as working electrode (W.E.), a standard saturated calomel electrode as reference electrode (R.E.) and a Pt plate as auxiliary electrode (A.E.). Meanwhile, Zn–Al–Cd, with a composition of (wt%) 0.12 Al, 0.0034 Pb, 0.0017 Cu, 0.0033 Cd, 0.0032 Fe, 0.0023 Sn and balance Zn, and Mg–Mn, with a composition of (wt%) 0.004 Al, 0.024 Zn, 1.3 Mn, 0.0032 Fe, 0.0023 Cu and balance Mg, were selected as SA. They were ground and polished with no rust on the surface and connected to the CS sample by a thin Cu wire, which was isolated with solution by tapes. In additional, the three-electrode electrochemical cell was also used to monitor the polarisation potential on the CS samples with 4000 points detected during the experiments under SA protection.

2.4 Surface Characterisation

M-N3D video microscopy and scanning electron microscopy (SEM) coupled with energy dispersive spectrometry (EDS) were employed to characterise the surface morphology and chemical composition.

3 Results and Discussion

3.1 Measurement of PMW in the O/W Fluids

Fluids with a water content of 45 % were chosen as the representative of the O/W fluids. The surface morphology and elements distribution of the CS samples under NP protection (SCE) of −0.3 V vs. open circuit potential (OCP) and SA of Mg–Mn and Zn–Al–Cd with an area ratio of 0.5 in salt-containing and salt-free fluids were detected.

3.1.1 NP Protection Method

Figure 2 shows the surface morphology views and EDS results of the CS samples under NP protection in the three kinds of oil–water fluids. Apparent corrosion occurred in the DW–oil fluid and corrosion was limited in the salt-containing fluids according to the macro-morphology views. Though the salt-containing fluid was conducive to inhibit corrosion under NP protection, corrosion was stilled detected in SEM views and EDS results.

Figure 3 displays the current density in the three-electrode circuit. The high solution resistivity in the salt-free fluid lowered the current density and induced large IR drop, which made the real protection potential on the CS sample not negative enough and thus could not protect the CS sample from corrosion as shown in Fig. 2d and g. Corrosion still remained in the salt-containing fluids according to the surface morphology analysis of the unworn

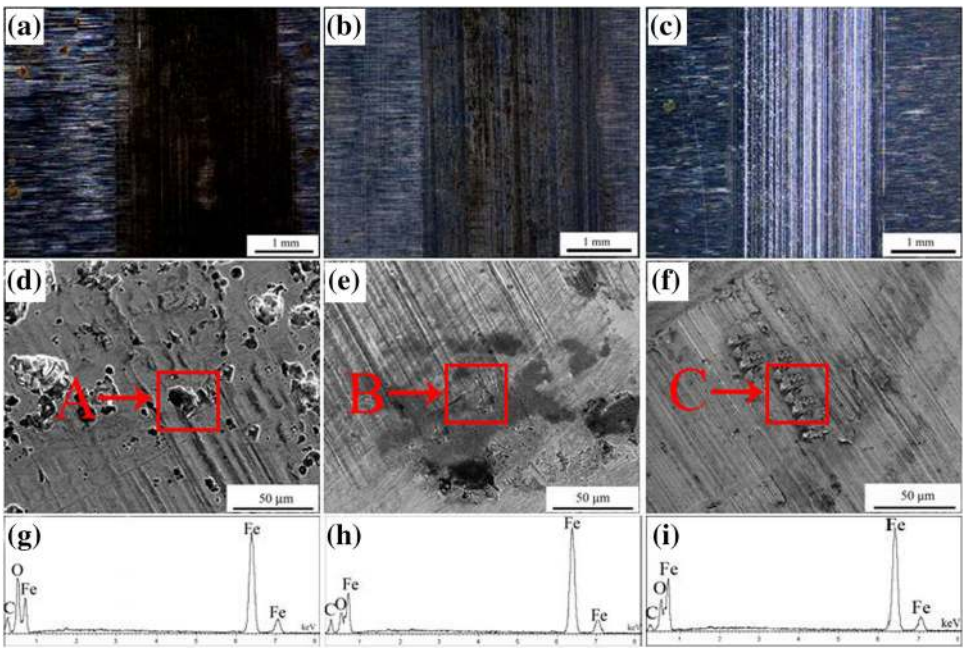

Fig. 2 Macro-morphology and SEM images of the unworn place of CS under NP protection, respectively, in **a** and **d** DW-, **b** and **e** NaCl-, **c** and **f** $NaHCO_3$-oil fluids with a water content of 45 %; EDS spectra obtained at **g** *A*, **h** *B* and **i** *C*

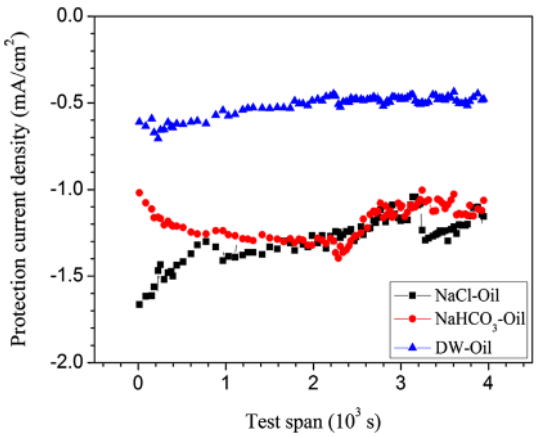

Fig. 3 Cathodic protection current density under NP protection in the O/W fluids with a water content of 45 %

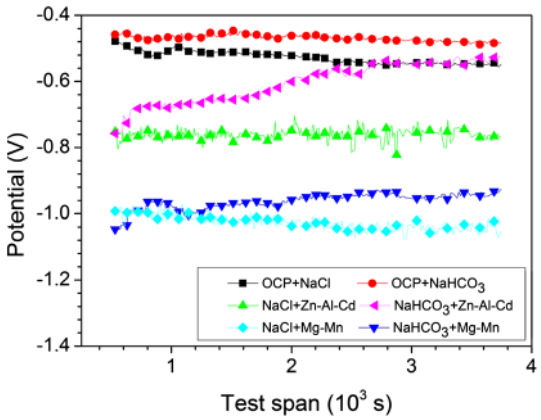

Fig. 4 OCP and the polarisation potential under SA protection of CS in the salt-containing fluids with a water content of 45 %

place and the elemental analysis as shown in Fig. 2e, f, h and i though the solution resistivity and IR drop both decreased.

The corrosion in the salt-containing fluid might be ascribed to the instability of the OCP of CS samples in the O/W fluids, as shown in Fig. 4. Under the NP protection, the protection potentials were applied according to the OCP detected before. However, the OCP changed when protection potentials were applied which would negatively or positively shift the protect potentials in comparison with −0.3 V and amplified the instability of the applied protection potentials in the O/W fluids, thus lowering the protection efficiency and causing corrosion.

The surface morphologies and EDS analysis of CS samples on the unworn locations under NP protection generally implied that the method used was not suitable for the PMW study of CS in oil–water fluid because of the unstable OCP.

3.1.2 SA Protection of Zn–Al–Cd

Figure 5 shows the macro-morphology views of the wear surface under the protection of Zn–Al–Cd. Serious corrosion occurred in the salt-free fluid and a yellow–brown layer existed on the CS sample surface in the $NaHCO_3$–oil fluid while the surface of the CS sample in the NaCl-containing fluid was smooth and clean.

It is well known that the OCP (E_{corr}) of the CS samples, which is between the anode equilibrium potential ($E_{(e,a)}$) and the cathode equilibrium potential ($E_{(e,c)}$), is a mixed potential of anode and cathode reactions on the CS surface. When the Zn–Al–Cd anode was connected with the CS sample, an extra cathodic current was employed on the CS sample. Consequently, the polarisation potential of the CS samples shifted negatively from E_{corr}, and the anodic current of the CS sample decreased. The CS samples could be perfectly protected from corrosion when the polarisation potential of the CS samples was lower than $E_{(e,a)}$.

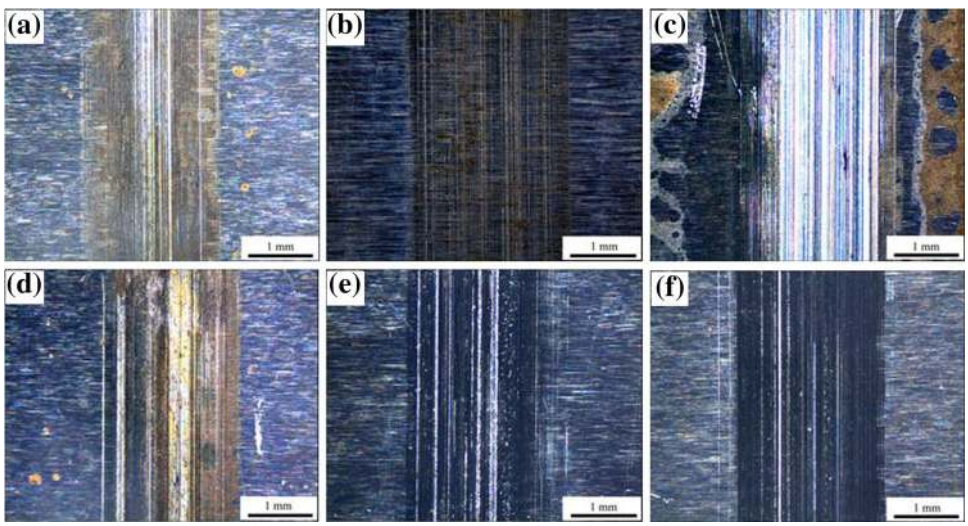

Fig. 5 Macro-morphology of CS under Zn–Al–Cd and Mg–Mn protection, respectively, in **a** and **d** DW-, **b** and **e** NaCl-, **c** and **f** $NaHCO_3$-oil fluids with a water content of 45 %

Table 1 Consumption of Zn–Al–Cd and Mg–Mn in the O/W fluids (mg)

Fluids	DW–white oil fluid	NaCl–white oil fluid	$NaHCO_3$–white oil fluid
Zn–Al–Cd	0.2	2.7	0.6
Mg–Mn	0.2	4.2	3.5

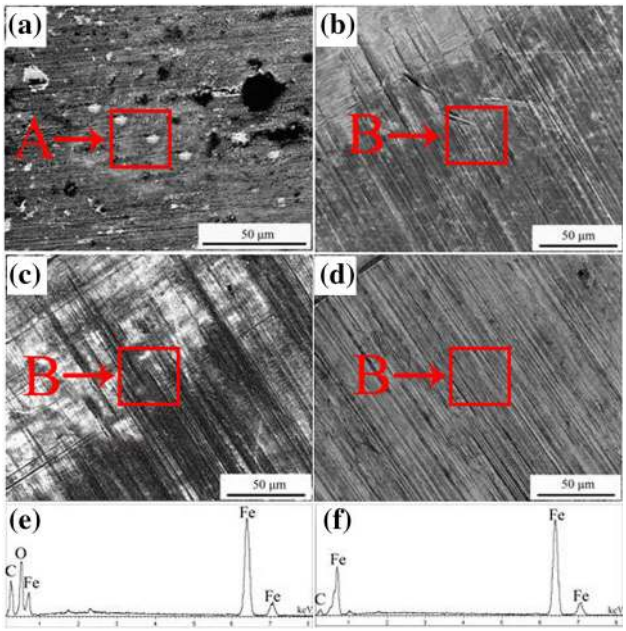

Fig. 6 SEM views of the unworn place of CS under Zn–Al–Cd and Mg–Mn protection, respectively, in **a** and **c** $NaHCO_3$-, **b** and **d** NaCl-oil fluids with a water content of 45 %; EDS spectra obtained at **e** *A* and **f** *B*

The consumption of Zn–Al–Cd was low in the salt-free fluid as shown in Table 1. The low consumption of Zn–Al–Cd in salt-free fluids could be attributed to the high solution resistance and the tendency of passivity of Zn–Al–Cd [21, 22]. As a result, Zn–Al–Cd could not provide enough cathodic current to polarise the CS potential beneath $E_{(e,a)}$ and decreased the protection efficiency of the anode.

The electrode potential of the CS sample in the NaCl-containing fluid was polarised down to approximately −800 mv (SCE) as shown in Fig. 4, owing to the cathodic protection current produced by Zn–Al–Cd anode. No corrosion was observed in the system of Zn–Al–Cd +NaCl-containing fluid in SEM views and EDS results shown in Fig. 6b and f. Thus, the system was suitable for the corrosion inhibition in the O/W fluid, and $E_{(e,a)}$ here must be above −800 mv (SCE).

The SEM views and elemental analysis of the yellow-brown layer on the CS unworn surface in the $NaHCO_3$-containing fluid in Fig. 6a and e demonstrated that serious corrosion happened because of the presence of O.

On one hand, the formation of $Zn(OH)_2{\cdot}ZnCO_3$ precipitation on the surface of Zn–Al–Cd [21] would decrease the consumption of SA and reduce the cathodic protection current. On the other hand, the decrement of protection current would accelerate the anodic polarisation of Zn–Al–Cd [21, 23]. Both the factors would low protection current and result in the positive shift of the electrode potential of the CS sample as shown in Fig. 4. The electrode potential of the CS sample almost approached the OCP and damaged the protection efficiency of Zn–Al–Cd. Consequently, corrosion still occurred in the Zn–Al–Cd + $NaHCO_3$ system.

According to the preceding analysis, corrosion could only be inhibited in the NaCl–containing O/W fluid under Zn–Al–Cd protection. And this system could be chosen as the cathodic protection method to study the PMW of CS here.

3.1.3 SA Protection of Mg–Mn

The macro-morphology views of the wear surface under Mg–Mn protection could also be seen in Fig. 5. The surface of the CS samples in the salt-containing fluids was smooth and clean, with no corrosion detected. By contrast, apparent corrosion was observed in the DW–white oil fluid. The salt-containing fluid was thus prior than the salt-free one to inhibit corrosion.

In the salt-free fluid, corrosion could not be inhibited under the protection of Mg–Mn because of the low dissolving rate of SA as shown in Table 1. In the salt-containing fluids, the high dissolving rate of Mg–Mn and the high driving voltage [21, 22, 24, 25] could generate enough protecting current to polarise the electrode potential beneath $E_{(e,a)}$ (Fig. 4) and maintain the CS sample in the protective potential region during the entire tests. Consequently, corrosion was relieved to the maximum extent. The alkaline atmosphere [21], which was beneficial to form precipitation film on the anode, should be responsible for the gradually decreasing of the protection current in the $NaHCO_3$-containing fluid.

SEM views and EDS results of the unworn surface of the CS samples in the salt-containing fluids was displayed in Fig. 6. The CS sample surfaces were smooth and clean, and the EDS spectrum gave the main elements of the CS with no corrosion. Therefore, the Mg–Mn anode was suitable to be used in the salt-containing fluid for the corrosion inhibition, in which the polarisation potential of the CS samples at −1000 mv (SCE) was competent to inhibit corrosion. According to the surface morphology and

elemental analysis, the CS sample could be protected from corrosion in the salt-containing fluid via Mg–Mn protection in the O/W fluids.

In summary, systems of Zn–Al–Cd + NaCl, Mg–Mn + $NaHCO_3$ and Mg–Mn + NaCl were competent to investigate the PMW behaviour in the O/W fluids due to their perfect corrosion inhibition. $E_{(e,a)}$ was more positive than −800 mv (SCE) and the polarisation potential range of −800 to −1000 mv (SCE) was proper to inhibit corrosion.

3.2 Measurement of PMW in Fluids Near PIP

The aforementioned three protection systems were utilised to discuss the PMW behaviour of CS in the oil–water fluid near PIP with a water content of 25 %. Figure 7 shows the surface morphology of the CS samples. Severe corrosion arose in the Zn–Al–Cd + NaCl system, pitting corrosion damage occurred in the Mg–Mn + NaCl system, and no corrosion or pit was observed in the Mg–Mn + $NaHCO_3$ system according to the macro-morphology.

Figure 8 displays the polarisation potential of the CS samples and the OCP in the salt-containing fluids obtained by the three-electrode system. All potentials were instable, which should be ascribed to the high instability of the fluid because of the frequent changing between W/O and O/W near PIP [17, 18, 20]. SA was not dissolved when oil wetting occurred on the surface. Hence, a change in flow patterns near PIP would result in the fluctuation and decrease of SA consumption rate, as shown in Table 2, which caused the fluctuation of the protecting current and the polarisation potential of the CS electrode.

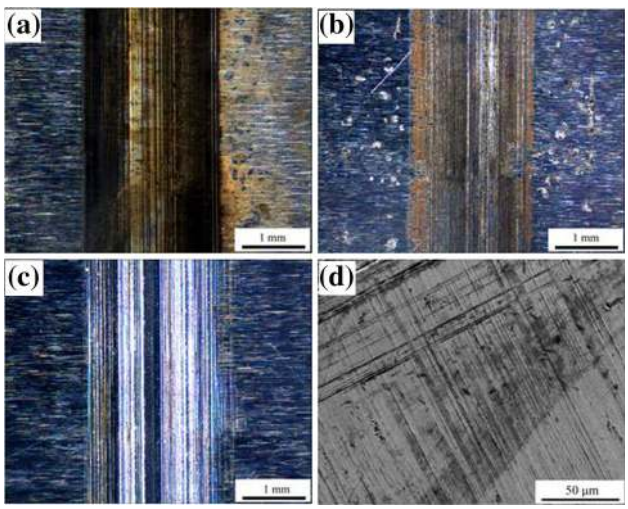

Fig. 7 Macro-morphology of CS in systems of **a** Zn–Al–Cd + NaCl **b** Mg–Mn + NaCl and **c** Mg–Mn + $NaHCO_3$ near PIP; **d** SEM image of CS in system of Mg–Mn + $NaHCO_3$

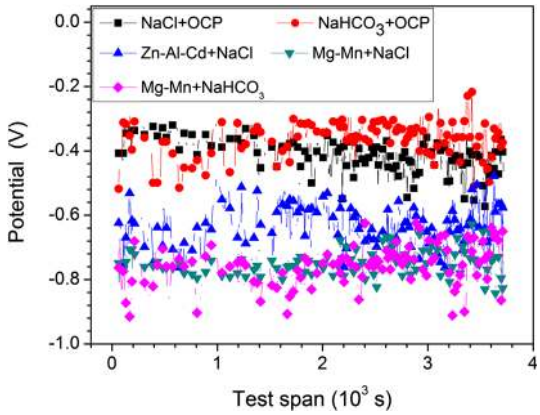

Fig. 8 OCP and Polarisation potentials under Mg–Mn protection of CS in fluids near PIP

In the Zn–Al–Cd + NaCl system, the polarisation potential of the CS sample was close to OCP as shown in Fig. 8. The decreased protecting current could not guarantee the polarisation potential of the CS samples beneath $E_{(e,a)}$ in the fluid near PIP, which should be the reason why serious corrosion still occurred under the protection of Zn–Al–Cd. The strong anode polarisation of Zn–Al–Cd caused by the drop of protection current density [21, 23] would narrow the driving voltage, thereby undermining the current efficiency. Therefore, discussing the PMW behaviour of CS in the NaCl-containing fluid under the protection of Zn–Al–Cd was inappropriate.

Figure 7b shows the surface morphology of the CS sample in the Mg–Mn + NaCl system. General corrosion was inhibited to some extent, but apparent pitting corrosion was detected. The high driving voltage and the consumption of Mg–Mn anode could generate enough cathodic current to protect the CS sample from serious corrosion. However, the violent fluctuation of the polarisation potential caused by the instability of cathodic protection current should be responsible for the serious pitting corrosion, especially in the fluid containing Cl^-. This finding was in accordance with the research of Cheng [26, 27], who also confirmed that the fluctuation of cathodic polarisation protection potential on the CS samples would trigger serious pitting corrosion with no passivity film.

In the Mg–Mn + $NaHCO_3$ system, no corrosion was detected because the micro-views of the unworn place was clean and smooth and the EDS results was the same to that in Fig. 6f, although polarisation protection potential fluctuation occurred. The existence of HCO_3^- and CO_3^{2-} could dutifully appease pitting corrosion by inhibiting the initiation and growth of pits [28, 29].

In general, the Mg–Mn sacrifice anode was not qualified for the PMW study of CS in the salt-free and NaCl-containing fluid because of serious corrosion and pitting

Table 2 Consumption of Mg–Mn in the fluids near PIP (mg)

Systems	Zn–Al–Cd + NaCl	Mg–Mn + NaCl	Mg–Mn + $NaHCO_3$
Weight loss (mg)	0.6	1.5	1

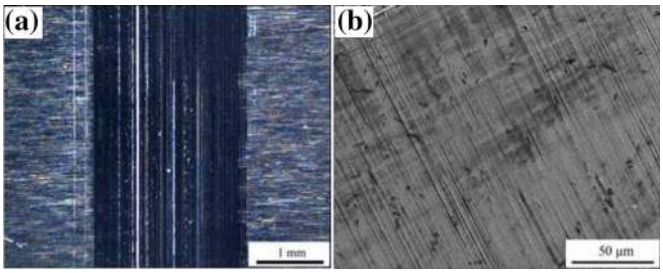

Fig. 9 **a** Macro-morphology and **b** SEM view of CS in the system of Mg–Mn + $NaHCO_3$ in the W/O fluids

corrosion while corrosion and pit nucleation were perfectly controlled in the $NaHCO_3$-containing fluid. Only the later system could thus be applied to discuss the PMW behaviour of CS in fluids near PIP.

3.3 Measurement of PMW in the W/O Fluids

The Mg–Mn + $NaHCO_3$ system was selected to investigate the PMW behaviour of CS in the W/O fluids, and the fluid with 5 % water component was selected.

The surface morphology in Fig. 9 shows the CS surface was clean and smooth with no corrosion, which demonstrated that the Mg–Mn anode was suitable to inhibit corrosion in the W/O fluid. The weak corrosive fluid and the alkaline environment should be commended for the excellent corrosion inhibition behaviour.

Overall, $NaHCO_3$ + Mg–Mn system was the optimal method to investigate the PMW component of the corrosive wear of CS in oil–water fluid through investigating the PMW of CS in three kinds of fluids. However, the area of SA significantly influenced the protective efficiency of SA protection, and the Mg–Mn anode exhibited a strong tendency of hydrogen generation with increasing SA area. Thus, the effect of the area ratio between the anode and CS sample on the PMW research in oil–water fluid is also important and worthwhile to inspect.

3.4 Effect of Area Ratio on PMW

Figure 10 displays the variation of weight loss of CS samples with an increment in area ratio. The weight loss increased before the area ratio came up to 2, and a small valley appeared at 4. The weight loss did not change much with the area ratio, except 0.5. And the polarisation potential of the CS samples shifted negatively and positively with the increasing of area ratio and testing span, respectively, as shown in Fig. 11.

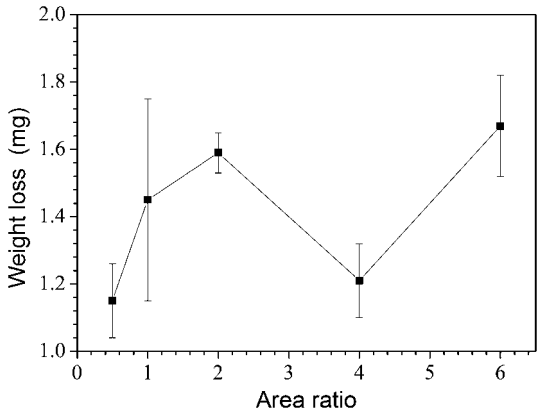

Fig. 10 Weight loss of CS with the increasing of area ratio in the O/W fluids

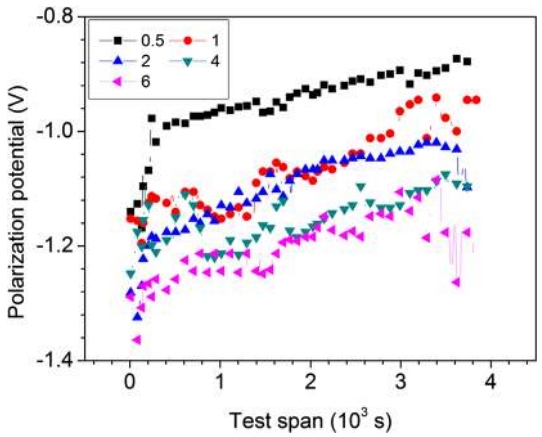

Fig. 11 Polarisation potential of CS with time at different area ratios in the O/W fluids

The consumption of SA increased with an increment of the area ratio, which would enhanced the protection current on the CS surface. The enhancement of protection current would launch much stronger cathodic polarisation on CS

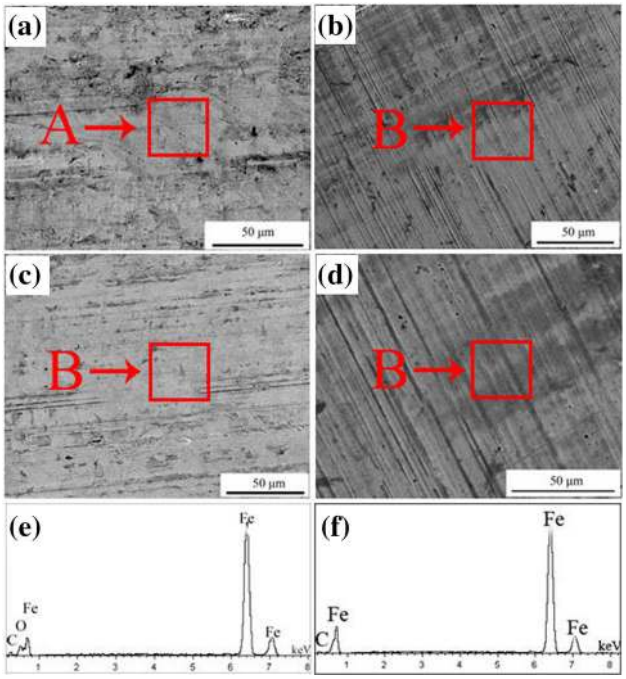

Fig. 12 SEM view of wear scar with area ratios of **a** 0.5, **c** 1 and the unworn place with area ratio of **b** 0.5 and **d** 1; EDS spectra obtained at **e** *A* and **f** *B*

and allow a more negative shift of the electrode potential of CS. But the precipitation of magnesium hydrate ($Mg(OH)_2$) would settle down on the surface of Mg–Mn little by little, which would decrease the consumption rate of SA [21, 22], decrease the protection current and induce a positive shift of the electrode potential of CS. In addition, the fluctuation of polarisation potential could be attributed to the instability of the fluid, especially near PIP.

Figure 12 displays the micro-views and EDS results. The surfaces of the unworn places and scars were all smooth and clean when the area ratios were 0.5 and 1. Oxygen was only inspected on the scar with an area ratio of 0.5. Considering that corrosion was controlled, oxygen could be generated by frictional oxidation in the scar because area ratio of 0.5 was too small to limit frictional oxidation. The protection of the frictional oxidation film could be a reason why the weight loss was low at an area ratio of 0.5 [3].

When the area ratio continued to increase, considerable debris was observed on the surface, as shown in Fig. 13. The debris should be ascribed to hydrogen embrittlement induced by the continuous negative shift of the cathodic polarisation potential on the CS samples [9, 12, 30, 31] with an increment in protection current. Hydrogen embrittlement would weaken the anti-wear capability of CS. Some large debris may be trapped in the scars when a large amount of debris was generated, and the trapped debris was rolled, oxidised and flattened there. During the experiment, hydrogen embrittlement enhanced weight loss and aggravated surface damage, whereas the trapping process would relieve the weight loss.

When the hydrogen generation process was not severe, the amount of debris trapped on the sample could compensate the weight loss and even cut down the weight loss. However, the weight loss would increase obviously as serious hydrogen embrittlement occurred. Clear evidence of hydrogen embrittlement was detected on the unworn locations when area ratio was more than 2 as shown in Fig. 14, where serious damage occurred with no corrosion product detected.

The area ratio would significantly affect the protection efficiency of the Mg–Mn anode generally. Frictional oxidation film would be generated when the area ratio was small, and the tendency of hydrogen embrittlement boosted with an enhancement in area ratio. The hydrogen embrittlement would improve weight loss but would reduce weight loss by enhancing the probability of debris trapping. Therefore, the PMW of materials should be determined by morphology and elemental analysis. Consequently, the area

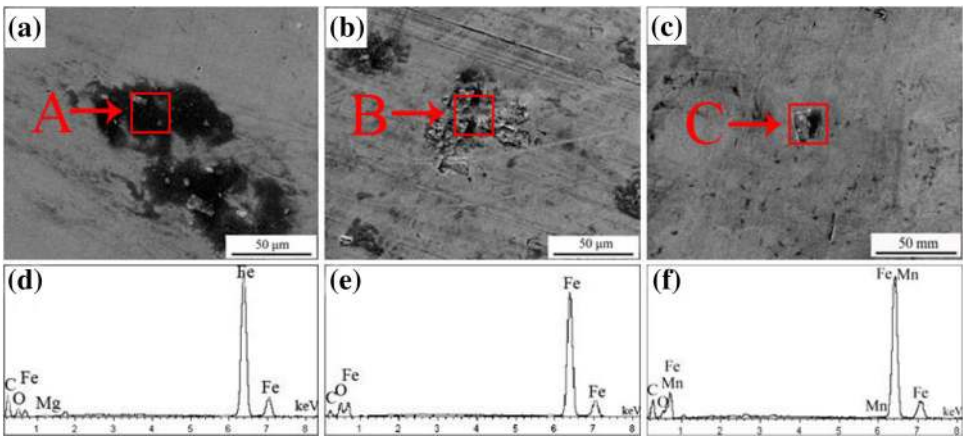

Fig. 13 SEM view of wear scar with area ratios of **a** 2, **b** 4 and **c** 6; EDS spectra obtained at **d** *A*, **e** *B* and **f** *C*

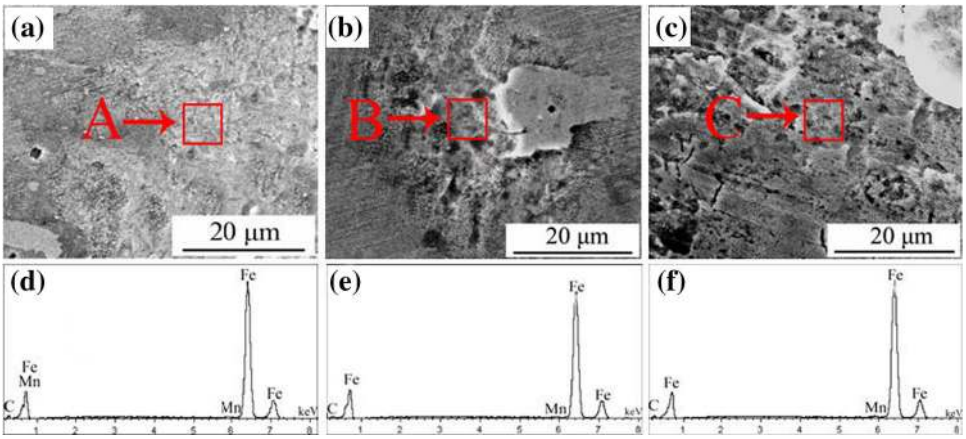

Fig. 14 SEM view of the unworn place with area ratios of **a** 2, **b** 4 and **c** 6; EDS spectra obtained at **d** *A*, **e** *B* and **f** *C*

ratio should be emphasised when SA was used to inhibit corrosion and it should not exceed 2 here.

4 Conclusions

The PMW behaviour of CS samples was investigated in three kinds of oil–water fluids. Surface morphology and elemental inspection were considered to determine the PMW measurement of CS in the oil–water fluids.

The NP protection method was not suitable to study the PMW of CS samples in oil–water fluids because of the unstable OCP of CS samples in the fluids. Zn–Al–Cd + $NaHCO_3$ and Zn–Al–Cd + NaCl systems were also not fitted to discuss the PMW of CS samples in oil–water fluids owing to the gradual anodic passivation of Zn–Al–Cd. Mg–Mn + NaCl could not inhibit the pitting corrosion of the CS sample in oil–water fluids, which resulted from the significant fluctuation of polarisation potential and the existence of Cl^-.

The Mg–Mn + $NaHCO_3$ system was the best way to evaluate the PMW of CS samples in oil–water fluids with different flow patterns because Mg–Mn could provide a high protection current, and HCO^{3-} and CO_3^{2-} could retard pitting corrosion. Meanwhile, the area ratio should be investigated because hydrogen embrittlement would occur when the area ratio was more than 2.

Acknowledgments Thanks for the financial support by The National Science Foundation of China (No. 51041007), The Tribology Science Fund of State Key Laboratory of Tribology of TsingHua University and The Graduate Innovation Fund of the Institute of Metal Research, Chinese Academy of Sciences.

References

1. Ko PL (1989) Reciprocating-sliding wear of sucker rods and production tubing in deviated oil wells. Wear 134:13–28
2. Chaoyang F, Jiashen Z (1998) Corrosion fatigue behavior of carbon steel in drilling fluids. Corrosion 8:651–656
3. Duan DL, Hu ZY, Jiang SL, Hou SH, Li S (2014) Corrosive wear behaviors of carbon steels in oil-water fluid. Tribol Trans 2:317–323
4. Assi F, Böhni H (1999) Study of wear–corrosion synergy with a new microelectrochemical technique. Wear 233–235:505–514
5. Hong MH, Pyun Sl (1991) Applied potential dependence of corrosive wear behaviour of 304-L stainless steel in sulphuric acid solution. J Mater Sci Lett 10:716–719
6. Zhang TC, Jiang XX, Li SZ (1996) Acceleration of corrosive wear of duplex stainless steel by chloride in 69 % H_3PO_4 solution. Wear 199:253–259
7. Akonko S, Li DY, Ziomek-Moroz M (2005) Effects of cathodic protection on corrosive wear of 304 stainless steel. Tribol Lett 18:405–410
8. Pamfilov EA, Prozorov YS (2012) On the modeling of mechanochemical wear. J Frict Wear 33:224–232
9. Jiang J, Stack MM, Neville A (2002) Modelling the tribo-corrosion interaction in aqueous sliding condition. Tribol Int 35:669–679
10. Guo HX, Lu BT, Luo JL (2005) Interaction of mechanical and electrochemical factors in erosion–corrosion of carbon steel. Electrochim Acta 51:315–323
11. Xu LY, Su X, Cheng YF (2013) Effect of alternating current on cathodic protection on pipelines. Corros Sci 66:263–268
12. Mischler S, Debaud S, Landolt D (1998) Wear-accelerated corrosion of passive metals in tribocorrosion systems. J Electrochem Soc 145:750–758
13. Huang Y, Jiang X, Li S (2000) Pure mechanical wear loss measurement in corrosive wear. Bull Mater Sci 23:539–542
14. Yaro AS, Hameed KW, Khadom AA (2013) Study for prevention of steel corrosion by sacrificial anode cathodic protection. Theor Found Chem Eng 47:266–273
15. Shehadeh M, Hassan I (2011) Study of sacrificial cathodic protection on marine structures in sea and fresh water in relation to flow conditions. Ships Offshore Struct 8:102–110
16. Mu H, Gong J, Chen J (2002) Phase transition process analysis of oil-water emulsion in horizontal tube. In: Chinese Society of Engineering Thermophysics, Bei Jing, pp 458–465
17. Wang AP (2011) Study on phase inversion of oil-water dispersion flow in horizontal pipelines. Dissertation, China University of Petroleum (East China)
18. Laflin GC, Oglesby KD (1976) An experimental study on the effect of flow-rate, water fraction and gas-liquid ratio on air-oil-water flow in horizontal pipes. Dissertation, The University of Tulsa

19. Angeli P, Hewitt GF (1998) Pressure gradient in horizontal liquid-liquid flows. Int J Multiph Flow 24:1183–1203
20. Lu YL, He LM, Wang AP (2011) Investigation of phase inversion in oil-water dispersed flow through horizontal pipe loop. J Petrochem Univ 6:79–83
21. Wu YS, Zheng JS (2005) The application technology of electrochemical protection and inhibition. Chemical Industry Press, Beijing
22. Baeckmann W, Schwenk W, Prinz W (1989) Handbook of cathodic corrosion protection, 3rd edn. VCH mbH press, Germany
23. Klein BB (1975) Ship electrochemical protection. National Defense Industry Press, Beijing
24. Chinese petroleum and natural gas industry (1998) Design specification of sacrificial anode for buried steel pipeline. Petroleum Industry Press, Beijing
25. JSPS Series (1972) Handbook of Metal Protection Technolog, New Edition edn. Nikkan Kogyo Shimbun, Tokyo
26. Liu ZY, Li XG, Cheng YF (2012) Understand the occurrence of pitting corrosion of pipeline carbon steel under cathodic polarization. Electrochim Acta 60:259–263
27. Liu ZY, Li XG, Cheng YF (2011) Electrochemical state conversion model for occurrence of pitting corrosion on a cathodically polarized carbon steel in a near-neutral pH solution. Electrochim Acta 56:4167–4175
28. Lou X, Singh PM (2010) Role of water, acetic acid and chloride on corrosion and pitting behaviour of carbon steel in fuel-grade ethanol. Corros Sci 52:2303–2315
29. Zhang BH, Cong WB, Yang P (2005) Electrochemical corrosion and protection of metals. Chemical Industry Press, Beijing
30. Cabrini M, Lorenzi S, Marcassoli P, Pastore T (2008) Effect of hydrogen diffusion on environmental assisted cracking of pipeline steels under cathodic protection. Metall Italiana 2:15–22
31. Zhang TC, Jiang XX, Li SZ (1997) Hydrogen-induced embrittlement wear of a high-strength, low-alloy steel in an acidic environment. Corrosion 53:200–205